Exact Coherent States: Importance & Identification

Rich Kerswell

Lectures 3 & 4

1 Importance of ECS

The importance of stable exact coherent structures (ECS) is obvious: they are attractors which attract all initial conditions in their basin of attraction. The importance of unstable ECS is more subtle yet can be no less significant. Although they are not asymptotic endstates, they influence the dynamics through their stable and unstable manifolds which may be quite global in phase space. ECS with only a small number of unstable directions (e.g 5 in a $O(10^5)$ dimensional phase space), act as focuses in phase space to which the flow is attracted along the (high-dimensional) stable manifold before ultimately being expelled out along the (very low dimensional) unstable manifold. If enough of these states exist together in phase space, this naturally gives rise to chaotic dynamics in which the flow trajectory travels between them like a ball in a pinball machine [10, 14, 15].

Given all the ECS which have now been found in pipe flow, an obvious thing to do is compare their physical properties with that of the transitional or turbulent state. Figure 1 plots the friction factor associated with each travelling wave (TW) together with that for the base parabolic state and the transitional state. The lower branch TWs have a friction factor generally closer to the base state whereas the upper branch TWs have a friction factor near and above the transitional flow value. Given this, it is clearly possible for a weighted sum of all the upper branch TW friction factors to produce a time-averaged value commensurate with the transitional value. Figure 1 and particularly the inset also clearly show the multiple saddle node bifurcations which occur as Re increases. It's worth remarking that the first ECS to be borne as Re increases appears at $Re = 773$ which is much lower than transitional turbulence which appears at $Re \approx 1800 - 2000$ (e.g. [18]).

[12] carried out particle image velocimetry of pipe flow for turbulent puffs ($1800 \lesssim Re \lesssim 2500$) and turbulent slugs for $Re \gtrsim 3000$ and found evidence for the transient realisation of TWs: see figure 2. This work has been repeated at $Re = 35,000$ to
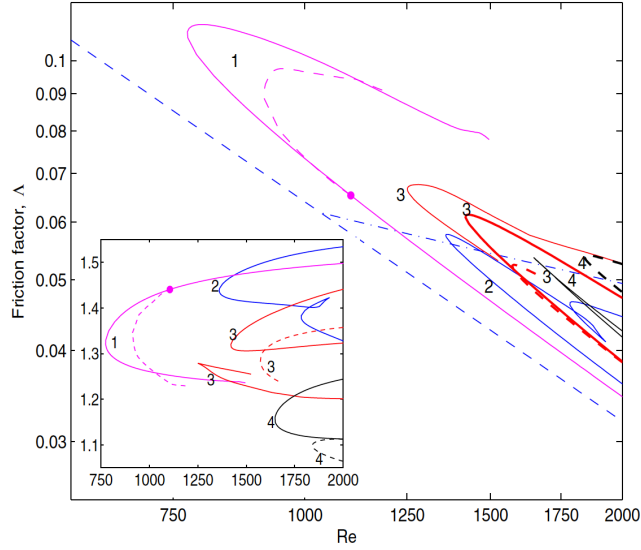
Figure 1: Friction factor Λ against Re for various TW families. The lower dashed line indicates the laminar value $\Lambda_{lam} = 64/Re$ and the upper dashed-dotted line the log-law parametrization of experimental data $1/\sqrt{\Lambda} = 2.0 \log(Re\sqrt{\Lambda})$. The labels show the rotational symmetry of the TWs (e.g. 3 means invariance under rotation by $2\pi/3$ around the pipe axis). The inset shows the phase velocity (in units of the mean bulk velocity) versus Re (this is figure 6 from [16]).
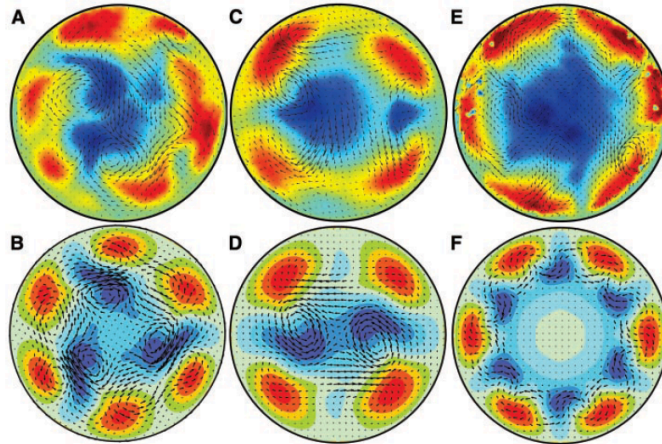
Figure 2: Comparison of experimentally-observed (top) and theoretically-calculated (bottom) streak patterns (red/blue colours indicate speeds faster/slower than the parabolic base profile). Velocity components in the plane are indicated by arrows. A is at $Re = 2000$, B is at $Re = 1250$, C is at $Re = 2500$, D is at $Re = 1360$, E is at $Re = 5300$ and F is at $Re = 2900$ (from [12]).

2

confirm this picture in fully turbulent pipe flow [6]. The same, of course, can be done for DNS of pipe flow turbulence. In [16], suitable indicator functions were developed to identify when an instantaneous velocity snapshot in such a DNS resembles a known TW. Figure 3 shows a good example of a near correspondence with a 2-fold rotationally symmetric TW. [16] estimated that an upper branch TW was visited in phase space for roughly 10% of time at $Re = 2400$. This sounds fairly low but crucially does not include other coherent structures like periodic orbits (see recurrent flow analysis below). [16] also explored the dynamics in the neighbourhood of the lower branch TWs by initiating DNS using a TW perturbed into the most unstable direction in its unstable manifold. Performing this in one sense (using an initial condition $\mathbf{u} = \mathbf{u}_{TW} + \varepsilon \mathbf{v}$ where $\mathbf{v}$ is the most unstable eigenfunction) led to the turbulent attractor while the other ($\mathbf{u} = \mathbf{u}_{TW} - \varepsilon \mathbf{v}$) caused the flow to smoothly relaminarise to the base state: see figure 4. This behaviour was found for all lower branch TWs tried indicating that they all sit in the laminar-turbulent boundary.
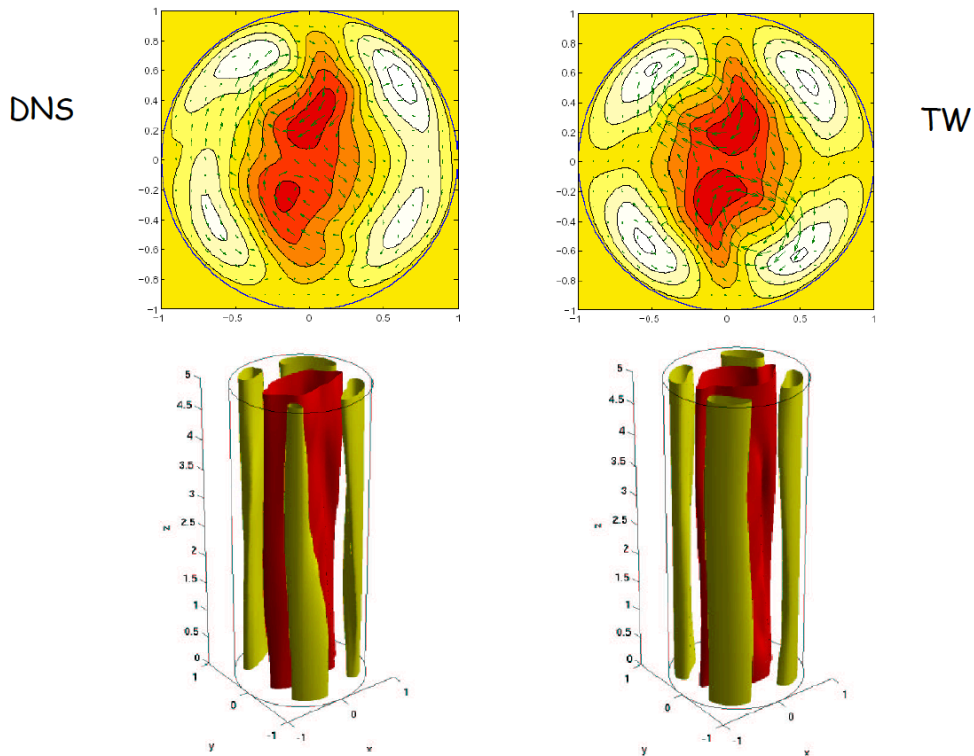
Figure 3: DNS of turbulent flow in a 5-diameter-long pipe transiently visits TWs. The plot on the left shows a DNS velocity field identified to resemble the TW on the right (cross-sections and full pipe images of the streamwise velocity anomaly are shown [16]).

3
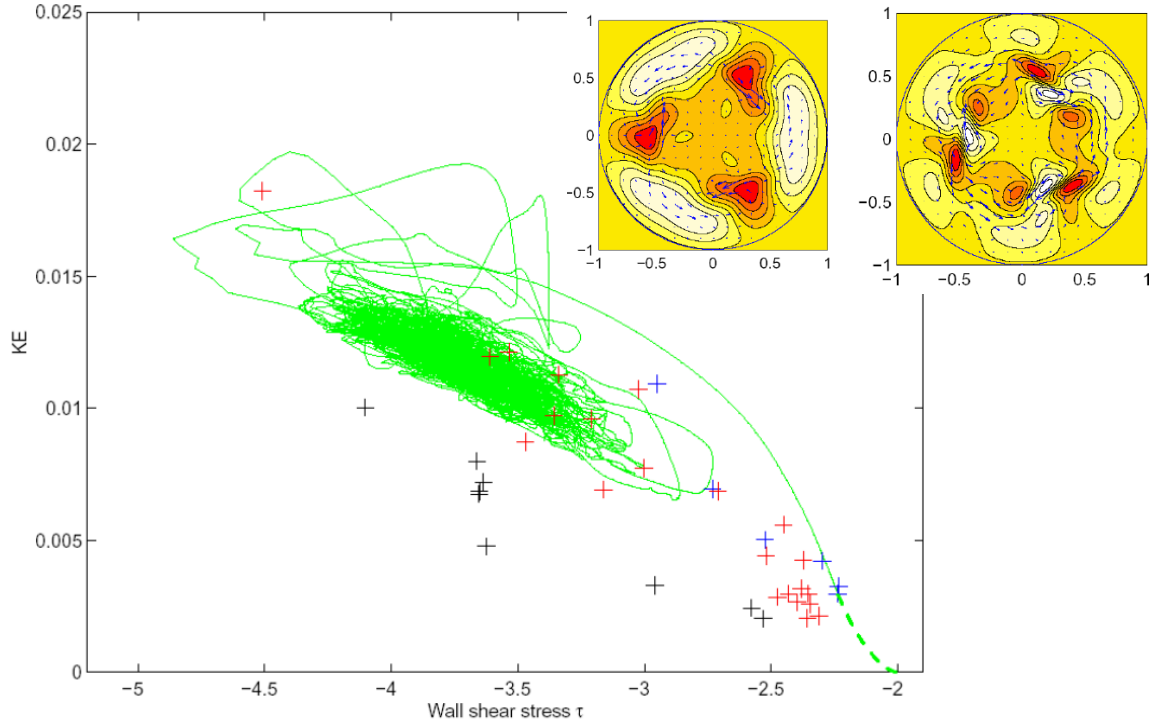
Figure 4: The perturbation kinetic energy of all the travelling waves (TWs) found in [28] plotted against their wall shear stress (so the laminar state $\mathbf{u}_{lam} := (1 - s^2)\hat{\mathbf{z}}$ is represented by the point $(-2, 0)$). TWs with 2-fold rotational symmetry are marked with blue+, 3-fold with red $+$ and, 4-fold with a black $+$. The green solid line is the result of starting a DNS run with a 2-fold TW $\mathbf{u}_{TW}$ and **adding** a small amount of its most unstable eigenfunction $\mathbf{v}$ whereas the dashed green line is the result of starting a DNS run with the same TW but now **subtracting** a small amount of $\mathbf{v}$. The former leads to turbulence and the latter smoothly relaminarises implying that the TW is embedded in the laminar-turbulent basin boundary. The inset shows a typical 3-fold rotationally symmetric TW on the left and its most unstable eigenfunction on the right: note how the eigenfunction is concentrated at a radius where the TW's shear is focussed (data from [16]).

Finally, [13] managed to discover a periodic orbit buried inside a turbulent attractor in small-box plane Couette flow: see the left plot in figure 5. The plot shown projects the turbulent DNS down onto an energy input rate I vs energy output (dissipation) rate D plane with the green dots indicating equally spaced points in time. The closed red loop is the periodic orbit (period 64.7 h/U where $2U$ is the differential speed between the planes and $2h$ is the separation between them) and the open yellow loop is that part of the DNS used as an initial guess to converge the periodic orbit. The plots on the right compare the mean flow and root mean square (rms) values of the fluctuation fields for the DNS (averaged over $6 \times 10^4 h/U$) and the periodic orbit.

4

The correspondence is astonishing (more on periodic orbits later).
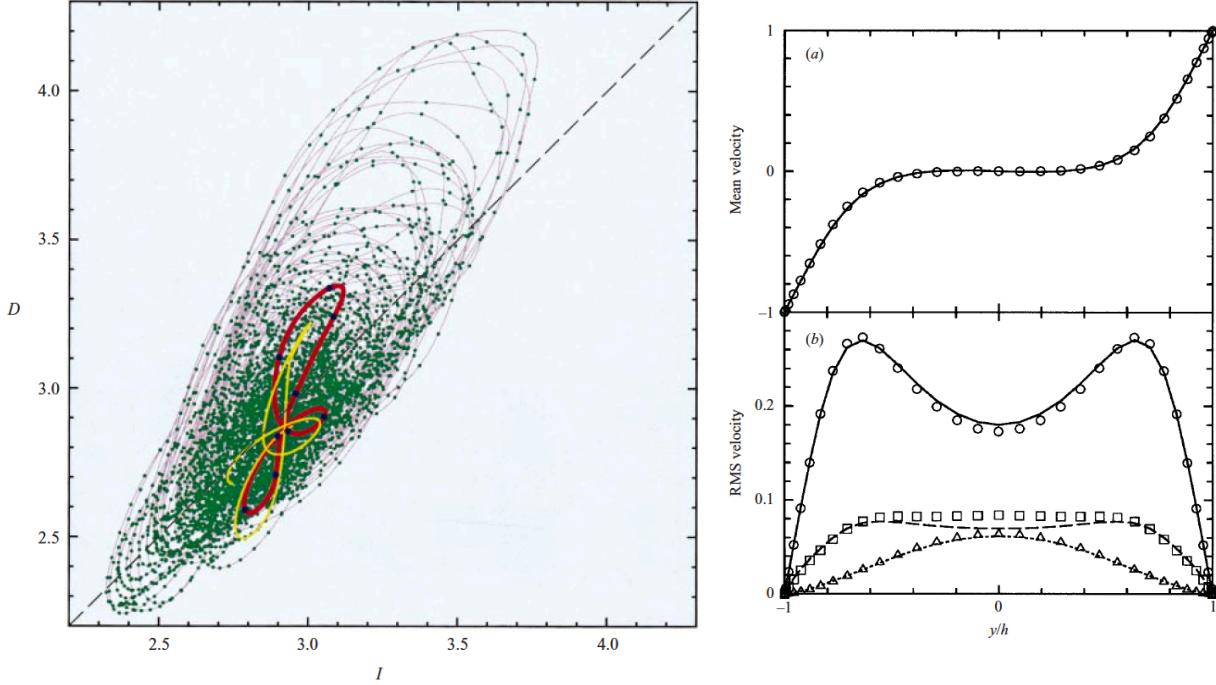
Figure 5: **Left**: Two-dimensional projection - dissipation rate D vs. energy input I - of a turbulent (grey line with green dots on equally spaced in time) and periodic orbit (closed red curve) in plane Couette flow over a domain $(L_x, L_y, L_z) = (5.5, 2, 3.8)$ at $Re = 400$, 15,000 degrees of freedom. The yellow open line is that part of the turbulent trajectory which closely shadows the red periodic orbit and provides the initial guess to converge the periodic orbit. **Right**: A comparison of the leading turbulent statistics and those of the periodic orbit (turbulent averages taken over $6 \times 10^4 h/U$ and $64.7 h/U$ for the periodic orbit) from [13].

2   Identification: Edge Tracking

We've already discussed homotopy as a means for finding ECS. Now we consider some alternative methods which have proved useful: edge tracking in this section and recurrent flow analysis in the next. Edge tracking can be a very useful technique for finding ECS in systems with bistability. Particularly important examples are shear flows where the base state is linearly stable yet a turbulent attractor also exists. Consider the simple 2D example

$$
\begin{aligned}
\dot{x} &= -x + 10y, \\
\dot{y} &= y(10e^{-0.01x^2} - y)(y - 1),
\end{aligned}
\tag{1}
$$

5

which has two stable equilibria and an unstable state. The line $y = 1$ separates
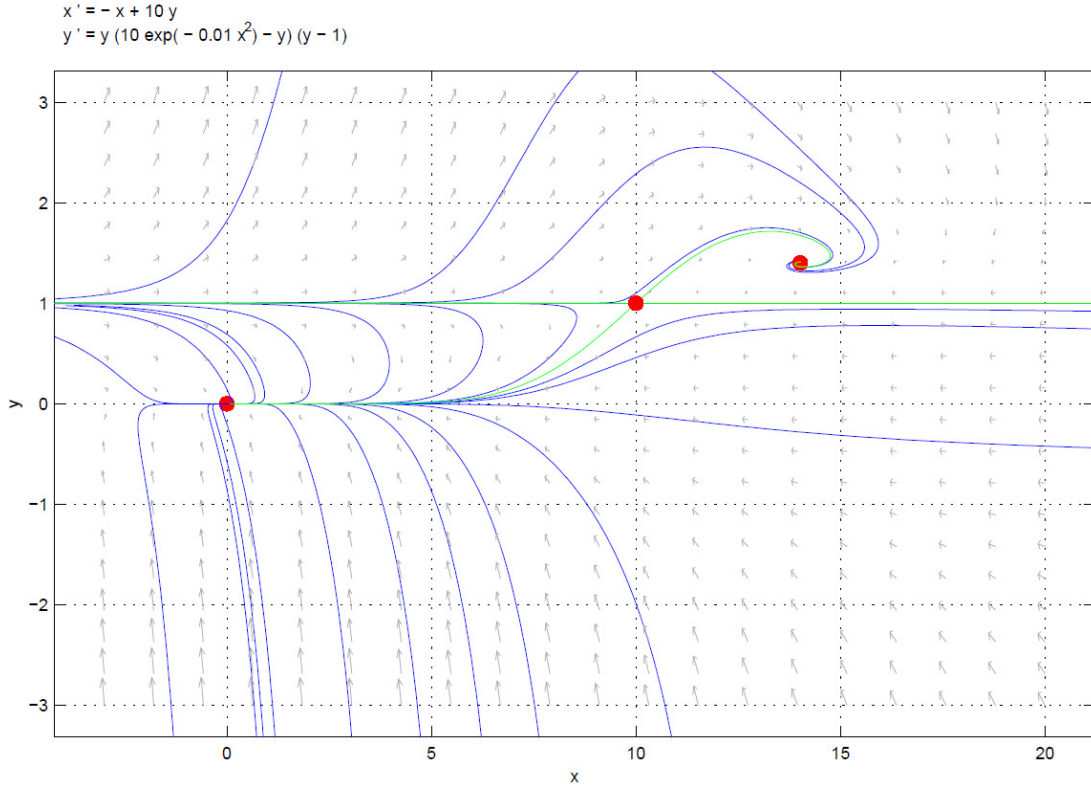
Figure 6: Phase plane of the 2D system (1) created using the free Matlab macro pplane6.m written by John Polking (Rice University, 1995). The laminar state is at $(0,0)$, the edge state at $(10,1)$ and the 'turbulent' state at $\approx (14,1.4)$. The edge is the line $y = 1$.

initial conditions which will laminarise to $(0,0)$ and those which become 'turbulent' by spiralling into the fixed point at $\approx (14,1.4)$: see figure 6. All points on $y = 1$ – here the basin boundary for the laminar and turbulent states or more generally called the 'edge' – are attracted to the relative attractor at $(10,1)$ which is called the 'edge state' (this is a saddle point in 2D but an attractor for trajectories confined to the 1D edge).

Edge tracking consists of a simple bisection procedure starting with a pair of initial conditions which are in different basins of attraction. By continuity, a line joining these initial conditions in phase space must cross the separatrix between the two basins so there must be at least one initial condition on this line which leads to neither attractor (i.e. it stays in the separatrix). Explicitly, let $u_0^{(n)}$ be the nth initial condition which leads to state 0 (i.e. $(0,0)$) and let $u_1^{(n)}$ be the nth to lead to state 1 (i.e. $\approx (14,1.4)$). The bisection procedure proceeds as follows: let $u := \frac{1}{2}(u_0^{(n)} + u_1^{(n)})$, find which basin u is in (so a time-stepper for the system is needed), then define a

new pair of initial conditions as follows

$$(u_0^{(n+1)}, u_1^{(n+1)}) = \begin{cases} (u_0^{(n)}, u) & \text{if} \quad u \to \text{state } 1 \\ \\ (u, u_1^{(n)}) & \text{if} \quad u \to \text{state } 0. \end{cases} \tag{2}$$

In our simple 2D example, we could take $u_0^{(0)} = (0, \frac{1}{2})$ and $u_1^{(0)} = (0, 2)$, then it's not hard to see that the bisection will lead to an interval converging around the point $(0, 1)$ which is on the separatrix and leads to the relative attractor - or *edge state* - $(10, 1)$.
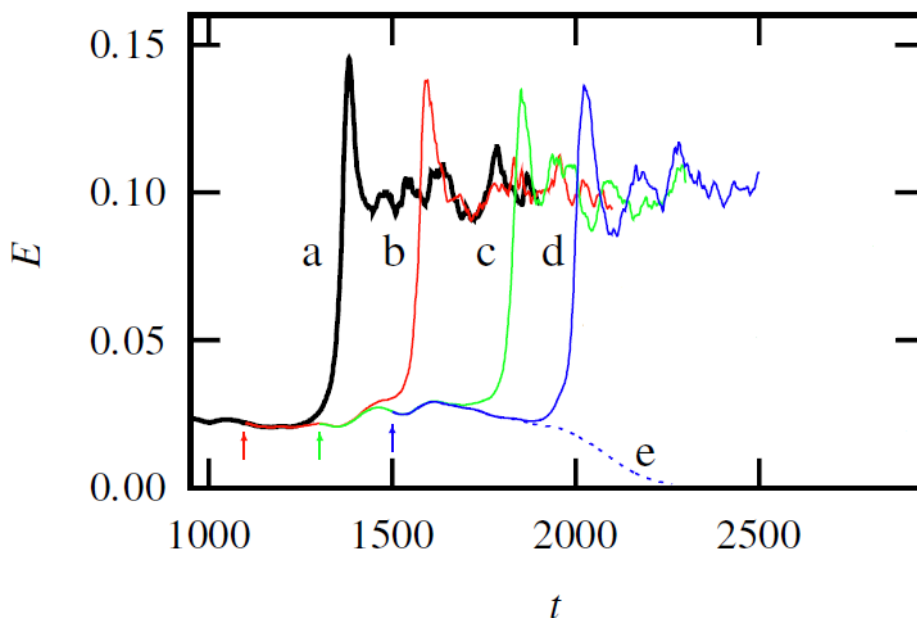
Figure 7: Perturbation energy traces of trajectories bounding the edge of chaos from [21]. Re=2875 and the pipe is $5\,D$ long.

This approach also works for the Navier-Stokes equations as first demonstrated by [25] and then performed for pipe flow by [21]. All that is required is an initial condition which triggers turbulence as the base state is clearly an acceptable initial condition which (trivially) leads to the base state. Figure 7 shows one of the edge trackings from [21] in a $5\,D$ pipe at $Re = 2875$. The first thing to notice is the characteristic way the trajectories leave the edge to swing up in energy to the turbulent state. The trajectory (d) and the relaminarising trajectory (e) both provide a good approximation to the edge dynamics until about $t \approx 1800$ when they start to separate. If the edge is followed for longer, chaotic dynamics are obtained as the 'edge state' (the limiting set).
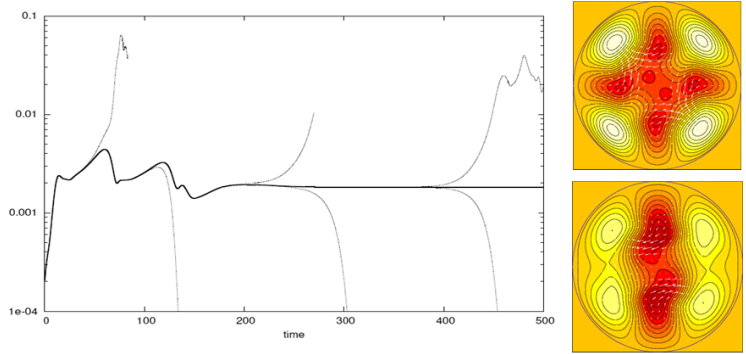
Figure 8: Edge tracking in pipe flow: energy contained in the axially dependent flow versus time. The thick line indicates the edge trajectory and the thinner lines nearby trajectories which either relaminarize (energy decrease) or become turbulent (energy increases to a higher level). Pipe length is 2.5 diameters, $Re = 2400$ and the flow is calculated within a 2-fold rotationally symmetric subspace (R_2-subspace in the notation of [9]). The two cross-sections on the right indicate (at least) two TWs which are stable on the edge (the upper one corresponds to the trace on the left at large times).
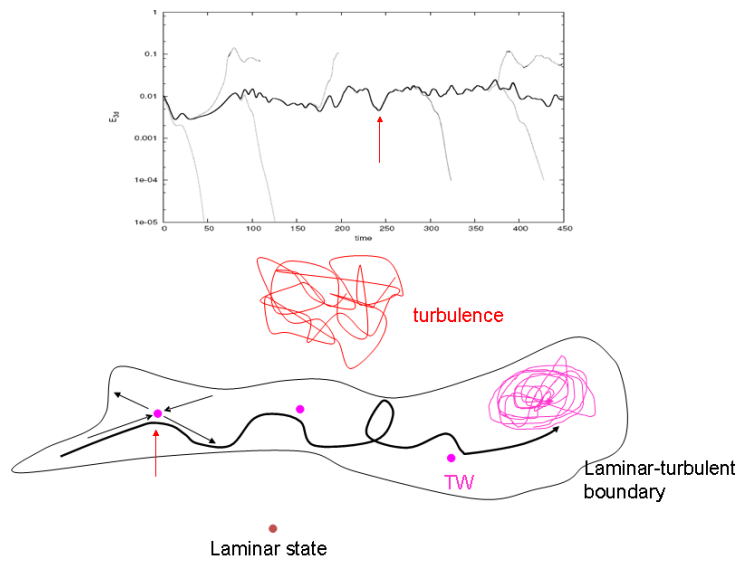
Figure 9: **Upper:** energy contained in the axially dependent modes on the edge for 5D pipe at $R_e = 2875$. The thick line indicates the edge trajectory. **Lower:** Schematic view of phase space. The surface separates initial conditions which relaminarize from those which become turbulent. An edge trajectory visiting three pink states is shown schematically [9].

Ideally, the edge state is an ECS and so the bisection procedure leads to a guess good enough for a Newton-Raphson solver, for example, to converge. If this doesn't occur initially, there is nothing to stop the procedure being repeated in a suitable subspace, for example, a 2.5 D-long pipe where the flow is forced to be symmetric

8

under a π rotation about its axis at $Re = 2400$ [9]. The plot of E_{3d} (energy in the streamwise-dependent part of the flow) as a function of time is shown in figure 8. The edge energy is seen to quickly level off indicating an edge state with *constant* E_{3d} which corresponds to a TW solution (labelled $C3\_1.25$ in [9] and later renamed $N2$ in [19]). This finding was significant in two ways. It was the first identification of a TW using this technique (see also [23] who found a steady state in small geometry plane Couette flow at about the same time) but it was not the expected TW. Calculations in [16] had identified that a lower branch TW (in their nomenclature $2b\_1.25$, now known as $S2$) only had one unstable direction indicating that this would be a relative attractor in the edge. However, the TW found possessed an additional mirror symmetry never seen before. Thus it was the first demonstration of multiple edge states. Secondly, the realisation that such 'highly symmetric' TWs could exist led to whole new families of TWs being quickly discovered thereafter [19]. As Re increases, these waves turn out to appear *before* the original less-symmetric TWs found in [11, 28]. These latter waves arise from the former in symmetry-breaking bifurcations ([19] shows an example of this - S3 bifurcating off N3 - in their figure 8).
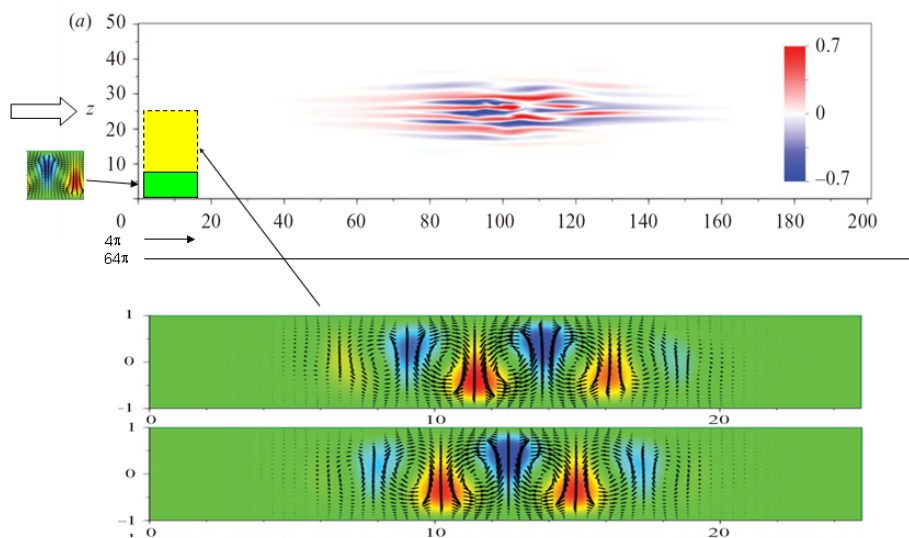
Figure 10: The small domain of [23] in which the edge state is a steady global state is shown as the lower left green rectangle (flow is left to right). The short wide box of [24] is shown as the lower left yellow rectangle (4 times wider than the green rectangle) with both dwarfed by the 16 times longer, wide box which captures a fully localised edge state [24]. Underneath are shown the spanwise localised states found by edge tracking in the short wide box.

[9] also noticed that the edge trajectory in the $5D$ case at $Re = 2875$ occasionally dipped to low energy values and smoothened locally (see Figure 8 for an example). They realised that the flows at these local energy minima turn out to be very close to other (lower branch) TWs embedded in the edge but these are now saddles there

rather than relative attractors. This clearly reinforces the picture of lower branch TWs embedded in the edge. The picture is then of the edge trajectory transiently visiting the neighbourhood of these (saddle) TWs before ultimately reaching an edge state (see figure 9).
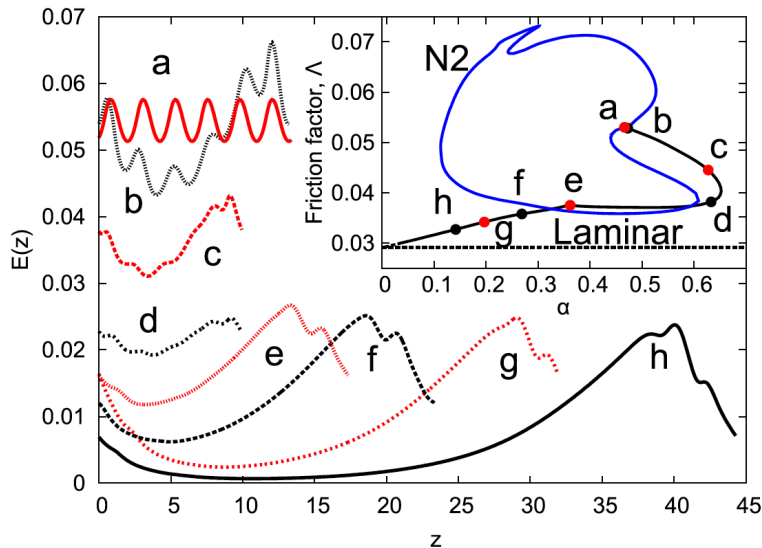
Figure 11: The birth of a localized TW in pipe flow from a bifurcation off the N2 TW [19] (3 copies in z). Main plot: $E(z) := \int_0^{2\pi} d\theta \int_0^1 s ds \frac{1}{2}\mathbf{u}^2$ demonstrating localization along the continuation curve. Inset: Continuation in $\alpha = 2\pi/L$ against the friction factor Λ. The branch moves towards smaller domains before turning in a saddle-node bifurcation and localizing. The friction factor's linear dependence upon α signals localization (from [4]).

2.1 Localized ECS

The bisection technique also works in larger geometries where the edge state turns out to be localised. In plane Couette flow, spanwise-localised equilibrium and travelling wave solutions were found [24] in short (streamwise) and wide (spanwise) domains. These spanwise-localised solutions were later found to bifurcate off the spanwise-periodic solutions already known [22] suggesting that all strictly periodic solutions could have connected localised versions too. Opening up the flow even further by considerably lengthening the domain leads to an edge state also localised in the streamwise direction, albeit now chaotic [7, 24]. Intriguingly, this edge state resembles a turbulent spot (although the energies are lower) and highlights the large size of domains needed to see streamwise localisation. Figure 10 illustrates this latter point by comparing the small plane Couette flow domain originally used for edge-tracking [23] ($4\pi \times 2 \times 2\pi$ being the streamwise, cross-stream and spanwise dimensions respectively) with the short, wide domain ($4\pi \times 2 \times 8\pi$) and long, wide domain ($64\pi \times 2 \times 16\pi$) of
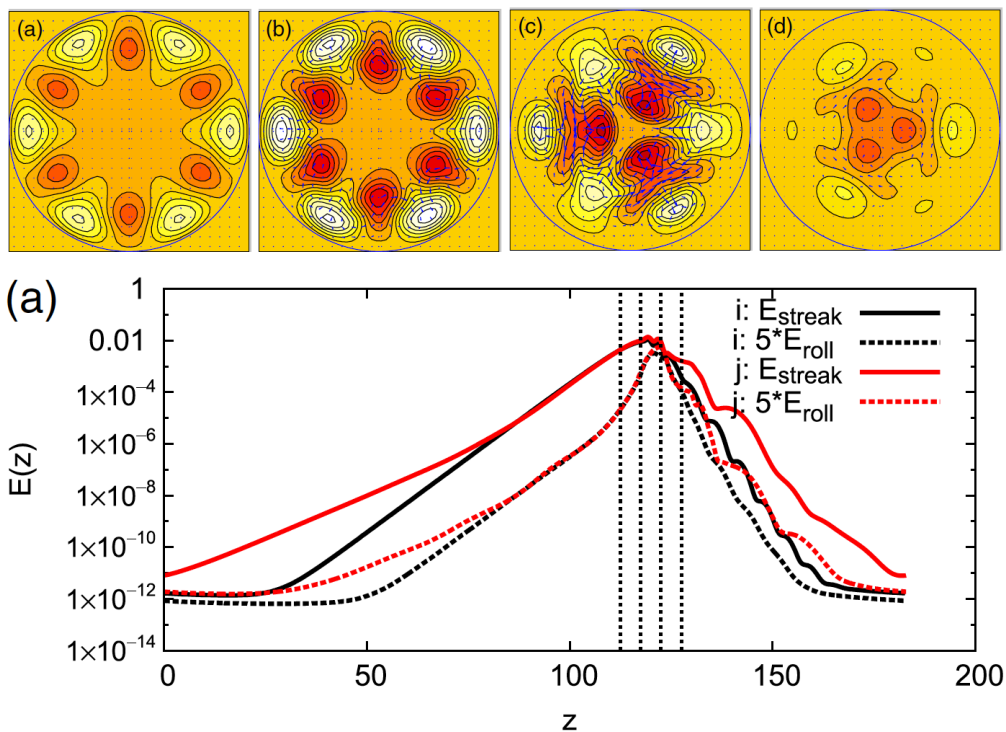
Figure 12: Energy in streaks and rolls as a function of downstream position z for two localized TWs in pipe flow (both invariant under a $2\pi/3$ axial rotation). Slices across solution i (black) are shown above (from [4]).

[24]. Localized ECS have also been found in channel flow [29], boundary layer flow [8] and pipe flow [1, 4]. The latter pipe flow study [4] traces a localized TW found by edge tracking back to find that it bifurcates off a global TW: see figures 11 and 12. Unfortunately, turning this process around, it is *a priori* unclear which bifurcations off the global TW will lead to localization without actually tracing them out.

3   Identification: Recurrent Flow Analysis

This is a fairly simple-minded technique to recognise nearly periodic motion in turbulent or chaotic flows. It has the considerable advantage over systematic bifurcation analysis in that any periodic orbits found have to be buried within the turbulent attractor and therefore dynamically relevant. This avoids the possibility of tracking Hopf bifurcations which turn out to be irrelevant for the turbulent flow. In 2001, [13] first showed that this can work for weakly-turbulent flows and it has been used and developed subsequently [27, 5, 3, 17].

11

In flows with net advection in one direction, periodic orbits, defined as

$$\mathbf{u}(\mathbf{x}, t+T) = \mathbf{u}(\mathbf{x}, t) \tag{3}$$

where T is the period, are actually rare. In this circumstance, the more common scenario is the existence of *relative* periodic orbits which recur after a time T but also with a shift $\boldsymbol{s}$ such that

$$\mathbf{u}(\mathbf{x}, t+T) = \mathbf{u}(\mathbf{x} + \mathbf{s}, t) : \tag{4}$$

see figure 13.
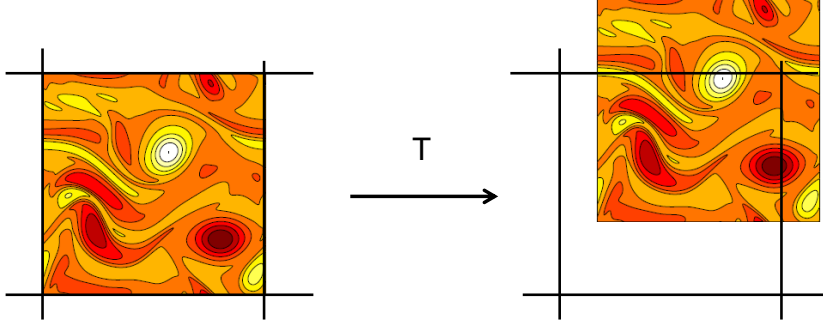
Figure 13: Relative periodic orbits: the flow recurs a time T later but with the the flow field shifted downstream (flow is left to right) and posssibly in the cross-stream direction too (the flow is periodic in both directions so repeats to fill the domain). A vorticity field is shown for illustrative purposes from 2D Kolmogorov flow [3]).

We use the context of 2D Kolmogorov flow - a flow over a 2D torus forced by a large-scale sinusoidal forcing - to illustrate recurrent flow analysis. Selecting a forcing with 4 wavelengths in the domain [3], the Navier-Stokes equations are

$$\frac{\partial \mathbf{u}^*}{\partial t^*} + \mathbf{u}^* \cdot \nabla^* \mathbf{u}^* + \frac{1}{\rho} \nabla^* p^* = \nu \nabla^{*2} \mathbf{u}^* + \chi \sin(8\pi y^*/L_y)\hat{\mathbf{x}} \tag{5}$$

where ρ is the density, ν the kinematic viscosity and χ is the forcing amplitude per unit mass of fluid over a doubly-periodic domain $[0, L_x] \times [0, L_y]$. The system is non-dimensionalised by the lengthscale $L_y/2\pi$ and timescale $\sqrt{L_y/2\pi\chi}$ so that the equations become

$$\frac{\partial \mathbf{u}}{\partial t} + \mathbf{u} \cdot \nabla \mathbf{u} + \nabla p = \frac{1}{Re} \nabla^2 \mathbf{u} + \sin 4y\hat{\mathbf{x}} \tag{6}$$

where the Reynolds number is

$$Re := \frac{\sqrt{\chi}}{\nu} \left(\frac{L_y}{2\pi}\right)^{3/2} \tag{7}$$

12

to be solved over the domain $[0, 2\pi/\alpha] \times [0, 2\pi]$ ($\alpha := L_y/L_x$). Given the doubly-periodic boundary conditions, dealing with the cross-plane vorticity equation is more natural and reduces simply to the scalar equation

$$\frac{\partial \omega}{\partial t} = -\mathbf{u} \cdot \nabla\omega + \frac{1}{Re}\nabla^2\omega - 4\cos 4y \tag{8}$$

where $\omega\hat{\mathbf{z}} := \nabla \times \mathbf{u}$. Dealing with this equation is analogous to working with the streamfunction $\mathbf{u} = \nabla \times \psi(x, y)\hat{\mathbf{z}}$ since spatially-constant velocity and vorticity fields are not present so $\psi = \nabla^{-2}\omega$. As always, knowing the symmetries of the problem is important. There is a *shift-&-reflect* symmetry

$$\mathcal{S} : [u, v, \omega](x, y) \to [-u, v, -\omega](-x, y + \frac{\pi}{4}) \tag{9}$$

which shifts half a wavelength of the forcing function in y and reflects in x ($\mathbf{u} := u\hat{\mathbf{x}} + v\hat{\mathbf{y}}$ and $\omega := \partial v/\partial x - \partial u/\partial y$). Since there are 4 wavelengths in the domain, this transformation forms a cyclic group of order 7. There is also a 2-fold rotational symmetry

$$\mathcal{R} : [u, v, \omega](x, y) \to [-u, -v, \omega](-x, -y) \tag{10}$$

and the continuous group of translations

$$\mathcal{T}_l : [u, v, \omega](x, y) \to [u, v, \omega](x + l, y) \qquad \text{for} \quad 0 \le l < \frac{2\pi}{\alpha}. \tag{11}$$

The vorticity is represented as follows

$$\omega(x, y, t) = \sum_{j=-N_x}^{N_x} \sum_{l=-N_y}^{N_y} \Omega_{jl}(t)e^{i(\alpha jx + ly)} \tag{12}$$

and we look for times t and values of $T \in \mathbb{R}$, $s \in [0, 2\pi/\alpha)$, $n \in \{0, 1\}$ and $m \in \{0, 1, 2, \ldots, 7\}$ for which

$$\mathcal{T}_s\mathcal{R}^n\mathcal{S}^m\omega(x, y, t+T) := \omega((-1)^{n+m}x + s, (-1)^n(y + m\pi/4), t + T) = \omega(x, y, t) \tag{13}$$

i.e. the vorticity field recurs up to the symmetry group of the system. The key to this search is to understand how approximately (13) should hold to signify the presence of a recurrent flow structure nearby. The only way to answer this seems to be to do computations and experiment. For simplicity in what follows, we assume henceforth that $n = 0$ and m is even (near recurrences with $n = 1$ or m being odd are 'pre'periodic to those with $n = 0$ and m and T doubled so in principle could still be detected - see [3]) The search for near recurrences then proceeds by seeking minima of the residual function

$$R(t, T) := \min_{0 \le s < 2\pi/\alpha} \min_{m \in 0,2,4,6} \frac{\sum_j \sum_l |\Omega_{jl}(t)e^{i\alpha js + iml\pi/2} - \Omega_{jl}(t-T)|^2}{\sum_j \sum_l |\Omega_{jl}(t)|^2} \tag{14}$$

13

over the (t,T) plane where $\sum_j \sum_l |\Omega_{jl}|^2 = \alpha/(4\pi)^2 \int_0^{2\pi/x} \int_0^{2\pi} \omega^2 dx dy$. There is a search over the continuous shift s here but, in practice, this is of course discretized over, say, 30 steps across the interval. A more elegant idea is to 'pull back' the state to a known reference point to compare states [2]. One way to do this is by shifting the state back until a chosen reference Fourier coefficient becomes purely real.
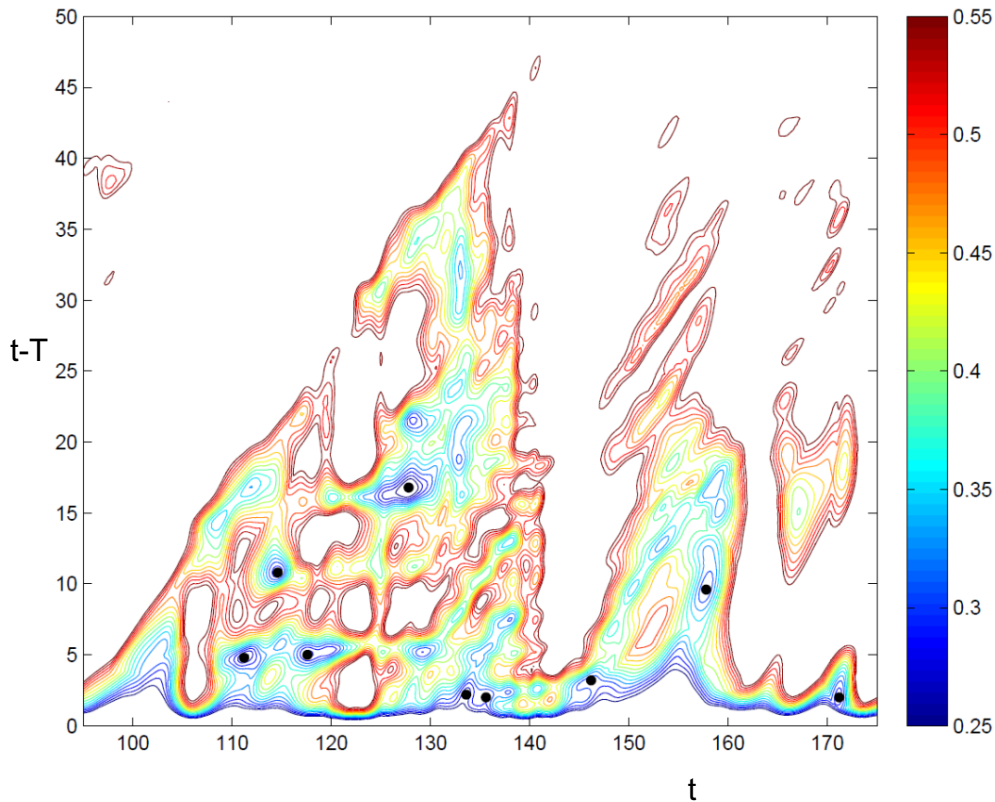
Figure 14: Example of $R(t,T)$ at $Re = 40$ in Kolmogorov flow contoured over $t \in [95, 175]$ (x-axis) and $T \in [thres, 50]$ (y-axis). The R values above 0.55 are not drawn for clarity (from [3]).

In terms of the 'history' over which to look, typically $0 < T_{thres} \approx 0.5 < T < 50$ where a threshold is necessary because $R(t,0) = 0$. Figure 14 is a typical example of how $R(t,T)$ looks as a function of t and T during a recurrent episode. The nine black dots are guesses identified by the code ($R < R_{thres} = 0.3$) over this time interval. All except one (the last dot at $t \approx 171$) subsequently converged to an exactly recurrent solution (the 4 dots for $t < 130$ to a periodic orbit with period 5.3807 and the next 4 dots with $t \in [130, 160]$ to a TW with phase speed $c = 0.0198$. The threshold R_{thres} needs to be chosen judiciously to give enough good quality guesses. Clearly the use of the L_2 norm in the residual definition is rather arbitrary and there are many opportunities to try to improve the accuracy of predicting a recurrent flow (e.g. see

14

[17]).

Once a near-recurrence has been found by the above stated criterion, a high-dimensional root finding algorithm is needed to try to converge this into an exactly recurrent state. To attempt this, a state vector is defined as

$$\mathbf{X} = \begin{bmatrix} \mathbf{\Omega} \\ s \\ T \end{bmatrix} \tag{15}$$

which contains information about the potential recurrence ($\mathbf{\Omega}$ is a vector containing the scalars Ω_{jl} arranged in some fashion). The shift s is included since it can be adjusted continuously whereas the discrete shift m cannot and therefore is pre-set. To set up the Newton-Raphson algorithm, it is convenient to define the infinitesimal generators $\mathcal{T}_x$ and $\mathcal{T}_y$ of translations in x and y respectively

$$\mathcal{T}_x\,\omega(x,y,t) \to \frac{\partial\omega}{\partial x} = \sum_{-N_y}^{N_y}\sum_{-N_x}^{N_x} i\alpha j\Omega_{jl}(t)e^{i(\alpha jx+ly)},$$

$$\mathcal{T}_y\,\omega(x,y,t) \to \frac{\partial\omega}{\partial y} = \sum_{-N_y}^{N_y}\sum_{-N_x}^{N_x} il\Omega_{jl}(t)e^{i(\alpha jx+ly)}$$

as they act in spectral space

$$\mathcal{T}_x\,\mathbf{\Omega} \to \mathbf{\Omega_x} \quad\text{and}\quad \mathcal{T}_y\,\mathbf{\Omega} \to \mathbf{\Omega_y} \tag{16}$$

where each element Ω_{jl} of $\mathbf{\Omega}$ is mapped to $i\alpha j\Omega_{jl}$ in $\mathbf{\Omega_x}$ and $il\Omega_{jl}$ in $\mathbf{\Omega_y}$. Then, in spectral space the recurrence condition (13) becomes

$$\mathbf{F}(\mathbf{\Omega}_0, s, T; m) := \exp(s\mathcal{T}_x + \tfrac{1}{4}\pi m\mathcal{T}_y)\hat{\mathbf{\Omega}}(\mathbf{\Omega}_0, T) - \mathbf{\Omega}_0 = \mathbf{0} \tag{17}$$

since, for example, $e^{s\partial_x}f(x) = f(x+s)$, where $\mathbf{\Omega}_0 = \mathbf{\Omega}(t)$ and $\hat{\mathbf{\Omega}} = \mathbf{\Omega}(t+T)$. If $\mathbf{X}_0 = (\mathbf{\Omega}_0, s_0, T_0)^T$ is an initial guess for a solution, then a better (next) guess $\mathbf{X}_0 + \delta\mathbf{X}_0 = (\mathbf{\Omega}_0 + \delta\mathbf{\Omega}, s_0 + \delta s, T_0 + \delta T)^T$ is given by

$$\frac{\partial\mathbf{F}}{\partial\mathbf{\Omega}_0}\delta\mathbf{\Omega} + \frac{\partial\mathbf{F}}{\partial s}\delta s + \frac{\partial\mathbf{F}}{\partial T}\delta T = -\mathbf{F}(\mathbf{\Omega}_0, s_0, T_0; m) \tag{18}$$

These are $\dim(\mathbf{\Omega})$ equations for $\dim(\mathbf{\Omega}) + 2$ unknowns. The extra two equations come from removing the degeneracy associated with these translational symmetries (the system is invariant under $(x,t) \to (x+s, t+T)$). This can be done by imposing that $\delta\mathbf{\Omega}$, has no component which shifts the solution infinitesimally in the x-direction

15

Figure 15: The dissipation D (normalized by the laminar dissipation) versus the energy input I (normalized in the same way) for a small number of recurrent flows uncovered at $Re = 40$ in 2D Kolmogorov flow. The shading is the p.d.f. of the turbulence found via direct numerical simulation (there are 11 levels 10^β with $\beta = -5, -4.5, \dots, -0.5, 00$ (from [3]).

or the $t-$direction (i.e. just redefines the time origin of the flow). The Newton-Raphson problem is then to solve

$$
\begin{bmatrix}
\ddots & & \vdots & \vdots \\
 & \dfrac{\partial \hat{\mathbf{\Omega}}_{\mathbf{s}}}{\partial \mathbf{\Omega}_0} - \mathbf{I} & \mathcal{T}_x\hat{\mathbf{\Omega}}_{\mathbf{s}} & \dfrac{\partial \hat{\mathbf{\Omega}}_{\mathbf{s}}}{\partial T} \\
 & \ddots & \vdots & \vdots \\
\cdots & (\mathcal{T}_x\mathbf{\Omega}_0)^T \quad \cdots & 0 & 0 \\
\cdots & \dfrac{\partial \mathbf{\Omega}_0}{\partial t}^T \quad \cdots & 0 & 0
\end{bmatrix}
\begin{bmatrix}
\vdots \\
\delta\mathbf{\Omega} \\
\vdots \\
\delta s \\
\delta T
\end{bmatrix}
= -
\begin{bmatrix}
\vdots \\
\mathbf{F}(\mathbf{\Omega}_0, s_0, T_0; m) \\
\vdots \\
0 \\
0
\end{bmatrix}
\tag{19}
$$

where $\hat{\mathbf{\Omega}}_{\mathbf{s}} := \exp(s\mathcal{T}_x + \frac{1}{4}\pi m \mathcal{T}_y)\hat{\mathbf{\Omega}}$ is the 'back-shifted' final state and $\mathbf{I}$ is the $\dim(\mathbf{\Omega}) \times \dim(\mathbf{\Omega})$ identity matrix. This is now in the standard form $\mathbf{A}\delta\mathbf{X} = \mathbf{b}$ with only the

16

Jacobian matrix $\partial\hat{\mathbf{\Omega}}_{\mathbf{s}}/\partial\mathbf{\Omega}$ not straightforward to evaluate ($\partial\hat{\mathbf{\Omega}}_{\mathbf{s}}/\partial T$ and $\partial\mathbf{\Omega}_0/\partial t$ are found by substituting $\hat{\mathbf{\Omega}}_{\mathbf{s}}$ or $\mathbf{\Omega}_0$ into the Navier-Stokes equations).
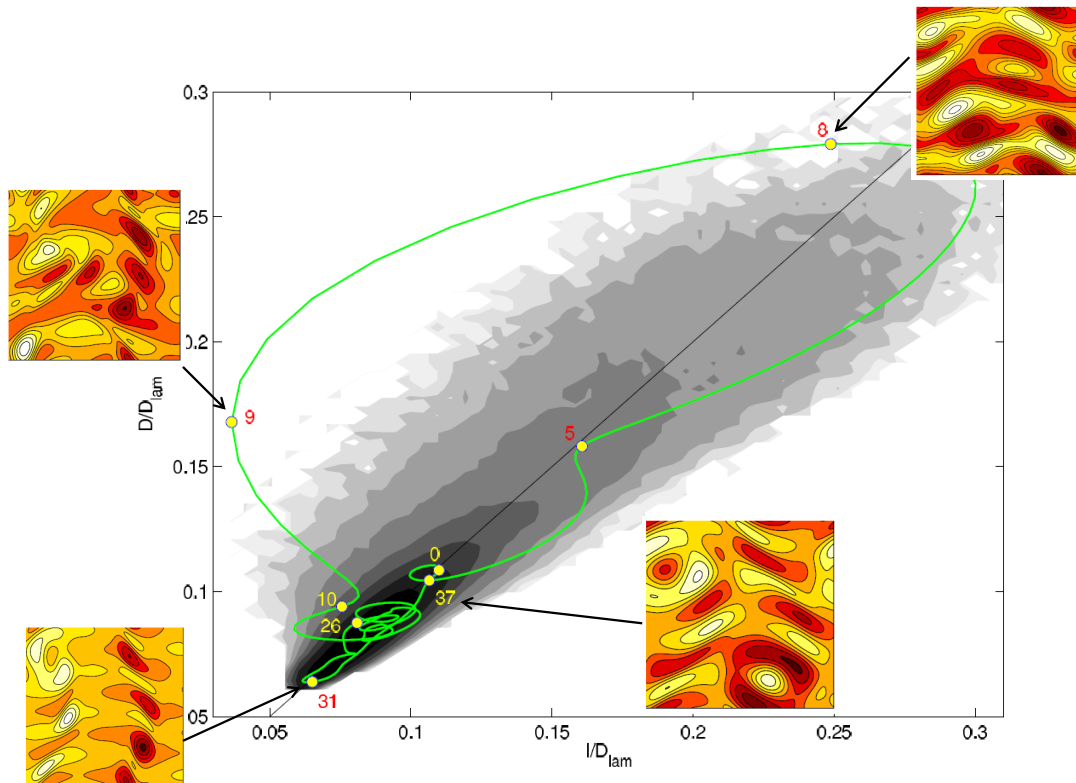
Figure 16: The dissipation D (normalized by the laminar dissipation) versus the energy input I (normalized in the same way) for the outer (magenta) recurrent flow in figure 15 (replotted here in green-sorry). Numbers indicate time along the orbit (period just over 37 time units) and velocity snapshots highlight the dynamics at different points long the period (from [3]).

Typically, the size of the matrix $\mathbf{A}$ is too large to store explicitly let alone attempt to solve $\mathbf{A}\delta\mathbf{X} = \mathbf{b}$ directly. As a result, the only way to proceed is iteratively and GMRES [20, 26]. Here only the effect of $\mathbf{A}$ on an arbitrary vector is needed. The effect of the troublesome Jacobian can be handled easily by a forward difference approach since

$$\frac{\partial\hat{\mathbf{\Omega}}_{\mathbf{s}}}{\partial\mathbf{\Omega}_0}\mathbf{y} \approx \frac{\hat{\mathbf{\Omega}}_{\mathbf{s}}(\mathbf{\Omega}_0 + \epsilon\mathbf{y}) - \hat{\mathbf{\Omega}}_{\mathbf{s}}(\mathbf{\Omega}_0)}{\epsilon} \tag{20}$$

where ϵ is chosen such that $||\epsilon\mathbf{y}|| = 10^{-7}||\mathbf{\Omega}_0||$ which balances truncation error with round-off error using double precision arithmetic and $||\cdot||$ is the Euclidean norm.

Figure 15 shows some recurrent flows found at $Re = 40$ in 2D Kolmogorov flow plotted on an energy out (dissipation rate) against energy input plot as in [13]'s original paper together with the pdf of the turbulent simulation data. The recurrent flows
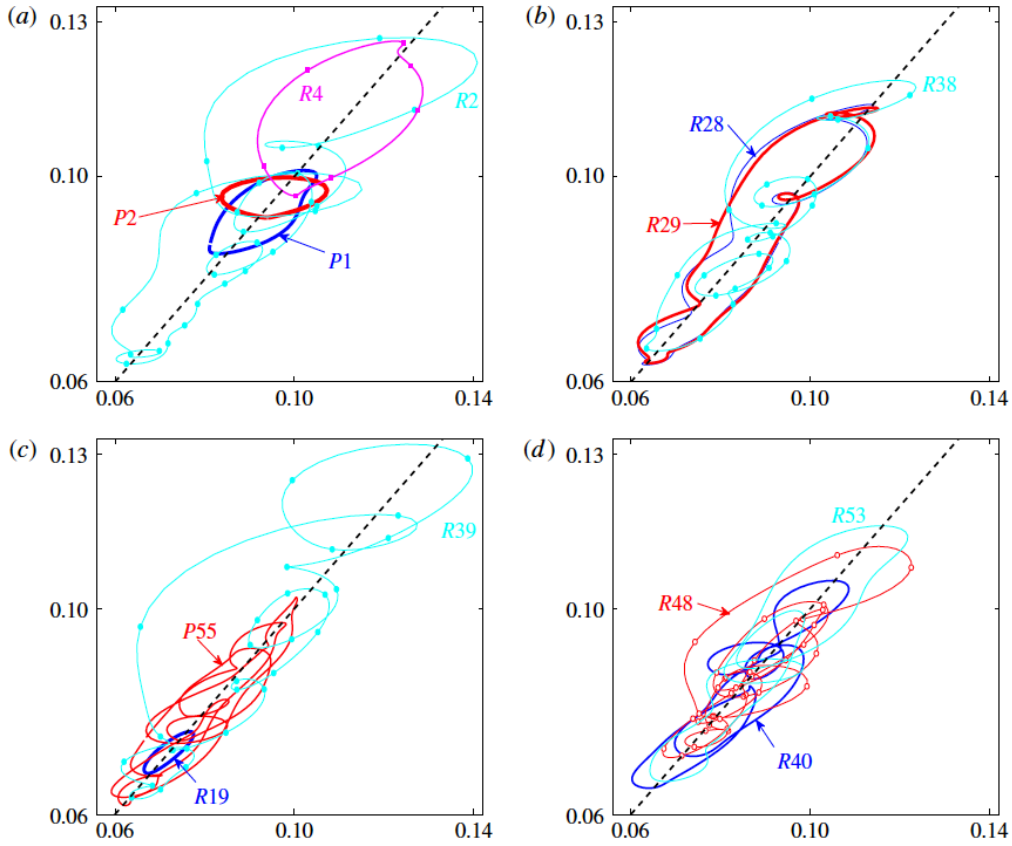
Figure 17: A sampling of recurrent structures found at $Re = 40$ plotted over the zoomed in box of figure 15. Symbols added to lines are to assist in their distinction and are spaced 1 time unit apart (nomenclature from [3]).

populate the heart of the pdf but some also capture infrequent but large excursions to high energy input and out rates. The outer magenta recurrent flow is shown in detail in figure 16 together with snapshots of the flow at certain times in its period. This sort of analysis can be useful for unfolding the dynamics underpinning the turbulence. Figure 17 zooms in on the dashed box drawn in figure 15 to show the variety of dynamics across a spectrum of recurrent flows (nomenclature from [3]). In figure 18, the part of the turbulent trajectory which was identified as showing nearly recurrent flow is reproduced next to the successfully-converged periodic orbit underpinning the behaviour. The final figure is from plane Couette flow [5]. Here the dynamics in 10^5 D is projected down to 3D in a way dependent on a frequently-visited equilibrium and its symmetric counterparts to most clearly display what is going on. What is interesting in this figure is how the five periodic orbits shown appear to marshal the turbulent trajectory in phase space.

18
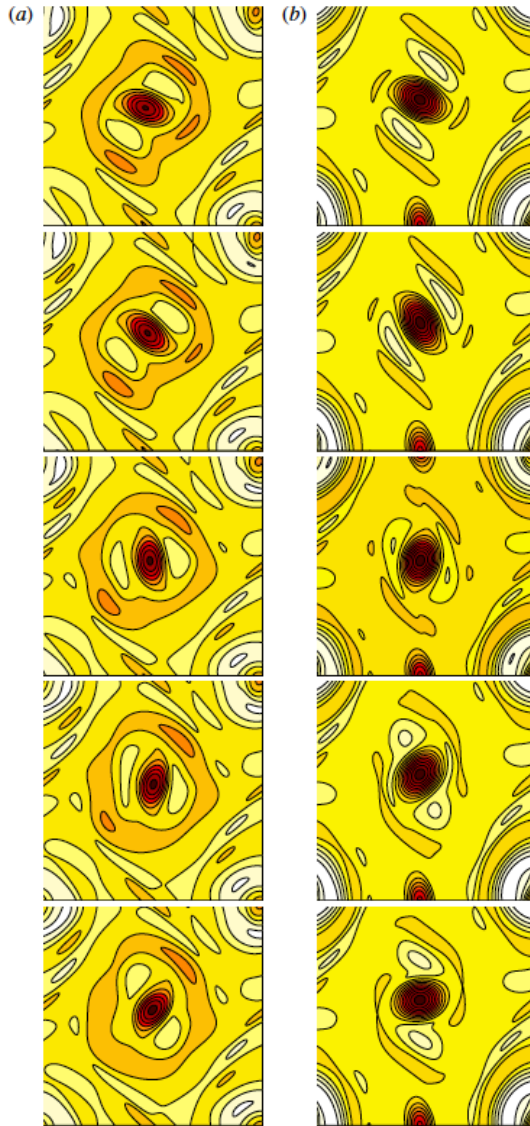
Figure 18: Part of the simulation trajectory (left) synchronized with the subsequently converged periodic orbit $P4$ (period 1.185) at $Re = 100$. The vorticity scale ranges from -26 (dark/red) to 12 (white). (Side-by-side videos are much better here - see lecture.

3.1   Summary

(i) ECS which are stable are important as they represent possible attractors of the dynamics. Unstable ECS can be just as important as they influence the dynamics through their stable and unstable manifolds. They have also been observed in experiments and numerical simulations albeit fleetingly.

(ii) In shear flows where the base state is linearly stable, ECS are born in saddle node

19
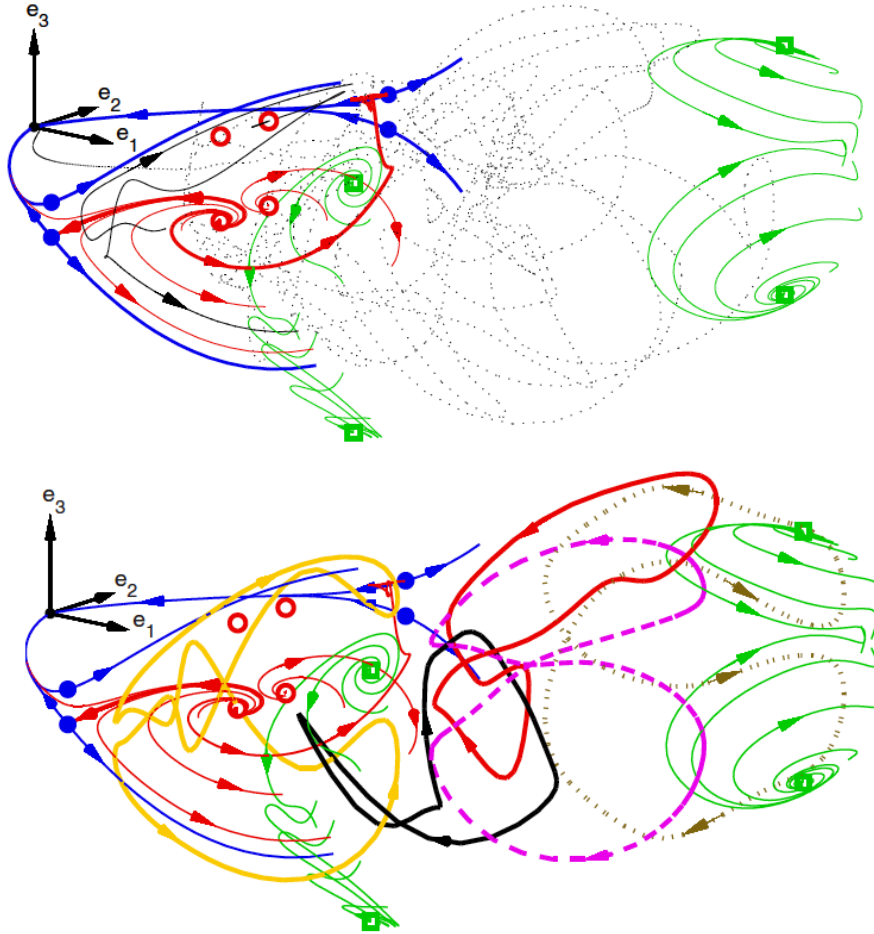
Figure 19: State-space projection from 10^5 D down to $3D$ (axes constructed from frequently visited ECS) for $Re = 400$ plane Couette flow. **Top**: several equilibria are indicated (circles, dots and squares), their unstable manifolds (lines enamating from symbols) and a typical turbulent trajectory (dotted). **Bottom**: five periodic orbits in the same state-space projection. These orbits capture well the coherent structures observed in the turbulent flow and appear to marshal the turbulent trajectory in state space. (from [5]).

bifurcations with the lower branch solutions embedded in the basin boundary of the base state. The corresponding upper branch states sit in the basin of attraction of the turbulent state and may even be embedded in the turbulent attractor itself.

(iii) Edge tracking is a useful method for studying the basin boundary between two attractors. At long times, edge tracking leads to a relative attractor on the 'edge' which may not be unique.

20

(*iv*) Recurrent flow analysis identifies nearly recurrent flow episodes in turbulent/chaotic dynamics which can then hopefully be converged to machine precision to relative periodic orbits of the Navier-Stokes equations. Although harder to perform, this technique has the desirable feature of always finding dynamically relevant ECS.

References

[1] M. Avila, F. Mellibovsky, N. Roland, and B. Hof, *Streamwise-localized solutions at the onset of turbulence in pipe flow*, Phys. Rev. Lett., 110 (2013), p. 224502.

[2] N. B. Budanur, P. Cvitanovic, R. L. Davidchack, and E. Siminos, *Reduction of SO(2) symmetry for spatially extended dynamical systems*, Phys. Rev. Lett., 114 (2015), p. 084102.

[3] G. J. Chandler and R. R. Kerswell, *Invariant recurrent solutions embedded in turbulent two-dimensional Kolmogorov flow*, J. Fluid Mech., 722 (2013), pp. 554–595.

[4] M. Chantry, A. P. Willis, and R. R. Kerswell, *Genesis of streamwise-localized solutions from globally periodic traveling waves in pipe flow*, Phys. Rev. Lett., 112 (2014), p. 164501.

[5] P. Cvitanovic and J. F. Gibson, *Geometry of turbulence in wall-bounded shear flows: periodic orbits*, Phys. Scr., 142 (2010), p. 014007.

[6] D. J. C. Dennis and F. M. Sogaro, *Distinct organizational states of fully developed turbulent pipe flow*, Phys. Rev. Lett., 113 (2014), p. 234501.

[7] Y. Duguet, P. Schlatter, and D. S. Henningson, *Localized edge states in plane Couette flow*, Phys. Fluids, 21 (2009), p. 111701.

[8] Y. Duguet, P. Schlatter, D. S. Henningson, and B. Eckhardt, *Self-sustained localized structure in boundary-layer flow*, Phys. Rev. Lett., 108 (2012), p. 044501.

[9] Y. Duguet, A. P. Willis, and R. R. Kerswell, *Transition in pipe flow: the saddle structure on the boundary of turbulence*, J. Fluid Mech., 613 (2008), pp. 255–274.

[10] B. Eckhardt, T. M. Schneider, B. Hof, and J. Westerweel, *Turbulence transition in pipe flow*, Ann. Rev. Fluid Mech., 39 (2007), pp. 447–468.

[11] H. FAISST AND B. ECKHARDT, *Travelling waves in pipe flow*, Phys. Rev. Lett., 91 (2003), p. 224502.

[12] B. HOF, C. W. H. VAN DOORNE, J. WESTERWEEL, F. T. M. NIEUWSTADT, H. FAISST, B. ECKHARDT, H. WEDIN, R. R. KERSWELL, AND F. WALEFFE, *Experimental observation of nonlinear travelling waves in turbulent pipe flow*, Science, 305 (2004), pp. 1594–1597.

[13] G. KAWAHARA AND S. KIDA, *Periodic motion embedded in plane Couette turbulence: regeneration cycle and burst*, J. Fluid Mech., 449 (2001), pp. 291–300.

[14] G. KAWAHARA, M. UHLMANN, AND L. VAN VEEN, *The significance of simple invariant solutions in turbulent flows*, Ann. Rev. Fluid Mech., 44 (2012), pp. 203–225.

[15] R. R. KERSWELL, *Recent progress in understanding the transition to turbulence in a pipe*, Nonlinearity, 18 (2005), pp. R17–R44.

[16] R. R. KERSWELL AND O. R. TUTTY, *Recurrence of travelling waves in transitional pipe flow*, J. Fluid Mech., 584 (2007), pp. 69–102.

[17] D. LUCAS AND R. R. KERSWELL, *Recurrent flow analysis in spatiotemporally chaotic 2-dimensional Kolmogorov flow*, Phys. Fluids, 27 (2015), p. 045106.

[18] T. MULLIN, *Experimental studies of transition to turbulence in a pipe*, Ann. Rev. Fluid Mech., 43 (2011), pp. 1–24.

[19] C. C. T. PRINGLE, Y. DUGUET, AND R. R. KERSWELL, *Highly symmetric travelling waves in pipe flow*, Phil. Trans. R. Soc., A 367 (2009), pp. 577–587.

[20] Y. SAAD AND M. H. SCHULTZ, *GMRES: A generalized minimal residual algorithm for solving non-symmetric linear systems*, SIAM J. Sci. Stat. Comput., 7 (1986), pp. 856–869.

[21] T. M. SCHNEIDER, B. ECKHARDT, AND J. A. YORKE, *Turbulence transition and the edge of chaos in pipe flow*, Phys. Rev. Lett., 99 (2007), p. 034502.

[22] T. M. SCHNEIDER, J. F. GIBSON, AND J. BURKE, *Snakes and ladders: localized solutions of plane Couette flow*, Phys. Rev. Lett., 104 (2010), p. 104501.

[23] T. M. SCHNEIDER, J. F. GIBSON, M. LAGHA, F. DE LILLO, AND B. ECKHART, *Laminar-turbulent boundary in plane Couette flow*, Phys. Rev. E, 78 (2008), p. 037301.

[24] T. M. SCHNEIDER, D. MARINC, AND B. ECKHART, *Localized edge states nucleate turbulence in extended plane Couette cells*, J. Fluid Mech., 646 (2010), pp. 441–451.

[25] S. Toh and T. Itano, *Low-dimensional dynamics embedded in a plane Poiseuille flow turbulence: travelling-wave solution is a saddle point?*, arXiv:physics/9905012, (1999).

[26] L. N. Trefethen and D. Bau, *Numerical Linear Algebra*, (1997).

[27] D. Viswanath, *Recurrent motions within plane Couette turbulence*, J. Fluid Mech., 580 (2007), pp. 339–358.

[28] H. Wedin and R. R. Kerswell, *Exact coherent structures in pipe flow: travelling wave solutions*, J. Fluid Mech., 508 (2004), pp. 333–371.

[29] S. Zammert and B. Eckhardt, *Streamwise and doubly-localized periodic orbits in plane Poiseuille flow*, J. Fluid Mech., 761 (2014), pp. 348–359.